International Symposium
On Turbulence and Shear Flow
Phenomena (TSFP-8)
August 28 - 30, 2013 Poitiers, France

GENERALIZED PHASE AVERAGING OF EXPERIMENTAL SURFACE-MOUNTED BODY WAKE MEASUREMENTS: 3D COHERENT STRUCTURES & DYNAMICAL MODELS

J. A. Bourgeois
Department of Mechanical and Manufacturing Engineering
University of Calgary
2500 University Dr NW, Calgary, AB T2N 1N4, Canada

B. R. Noack
Département Fluides, Thermique, Combustion
Institut PPRIME
43 rue de l'Aérodrome, F-86036 POITIERS CEDEX, France

R. J. Martinuzzi
Department of Mechanical and Manufacturing Engineering
University of Calgary
2500 University Dr NW, Calgary, AB T2N 1N4, Canada
rmartinu@ucalgary.ca

ABSTRACT

A six-dimensional model is proposed as a low-order representation of the vortex dynamics in the turbulent wake of a wall-mounted square-cross-section cylinder of height-to-width ratio $h/d = 8$ with one face normal to the flow at a nominal Reynolds number of 12,000. The wake flow is experimentally investigated for two oncoming turbulent boundary layers of thickness $\delta/d = 0.72$ and 2.6 using simultaneous planar PIV and surface pressure measurements. A novel generalized phase averaging technique is used to determine global harmonic and shift modes, representing the shedding instability and low-frequency behaviour, respectively. The generalized phase average provides a parametrization of the phase as well as the oscillation amplitude and base flow drift. Using this technique, two distinct coherent structure topologies are found, depending on δ/d, distinguished by the topology of the stream/cross-streamwise vortical strands giving rise to half-ring and full-ring structures for the thinner and thicker boundary layer, respectively. A six-dimensional model is derived where the state of the system, $\mathbf{f}(\mathbf{a}(t), \xi(t))$, depends on the vector of mode amplitudes, $\mathbf{a}(t)$, and a stochastic term, $\xi(t)$, simulating higher order contributions.

BACKGROUND

Many turbulent flows display oscillatory coherent structures with low frequency base flow drifts and modulation of the oscillation amplitude. Examples include vortex shedding behind bluff bodies (Williamson, 1996), helical vortices in swirling jets (Oberleithner *et al.*, 2011), Kelvin-Helmholtz structures in mixing layers (Liu, 1989), and Rossiter modes in cavities (Rowley & Williams, 2006). A classical approach for educing the coherent structures in such flows is a triple decomposition of the velocity field in a mean, a coherent (constant amplitude and frequency) and an incoherent (unresolved) component. The traditional phase average, however, lacks an account of the temporal variations of the oscillation amplitude and the low frequency drifts of the base flow. These two phenomena are intimately coupled, as has been described for laminar vortex shedding (Noack *et al.*, 2003), and remain so under fully turbulent conditions (shown herein). These two low frequency aspects are incorporated into a novel generalized phase average decomposition described in Bourgeois *et al.* (2013), whereby planar velocity POD modes determine global harmonic and shift modes, representing the shedding instability and the base flow slow-drift behaviour.

The case investigated is the wake of a relatively tall, wall-mounted bluff body protruding a nominally thin turbulent boundary layer. Two different mean wake flow topologies have been reported: either a single pair of counter-rotating streamwise trailing vortices extending from the free-end or two pairs extending from the free-end and body-wall junction. This change in mean flow topology has been related to the obstacle height-to-width aspect ratio, h/d, for circular (Sumner *et al.*, 2004) and square (Wang *et al.*, 2009; Bourgeois *et al.*, 2011) section cylinders. Herein, the aspect ratio is held constant while the boundary layer thickness, δ/d, is varied to show similar changes in mean topological structure. Instantaneously, highly three-dimensional coherent vortex structures are shed quasi-periodically which display corresponding differences in topology. The turbulent vortex shedding that occurs displays a high degree of amplitude and base flow modulation, making a traditional phase average inadequate to describe the flow dynamics.

This paper proposes to investigate these dynamics. Using the generalized phase averaged planar field, the 3D coherent structure construction is realized by correlating surface pressure and planar modal coefficients. A six-dimensional model is derived based on the most energetic modes and a stochastic-deterministic term simulating higher-order contributions.

GENERALIZED PHASE AVERAGING

In order to increase the fidelity of dynamical representation, generalized phase averaging (Bourgeois *et al.*, 2013) was introduced as a triple decomposition accounting for time variations of the base flow and the amplitude of coherent oscillations. This formulation is a more robust representation of the dynamic coherent structure behaviour than the traditional phase average. While the latter takes the base flow and oscillatory mode amplitudes to be constant in time, the generalized phase average incorporates temporal variations of both. Figure 1 presents the data reduction procedure where the velocity, $\mathbf{u}(\mathbf{x},t)$, is decomposed as

$$\mathbf{u}(\mathbf{x},t) = \mathbf{u}_B(\mathbf{x},t) + \mathbf{u}_\phi(\mathbf{x},t) + \mathbf{u}_S(\mathbf{x},t) \tag{1}$$

The base flow, $\mathbf{u}_B(\mathbf{x},t)$, is the sum of the long-time mean, $\mathbf{U}$, and shift mode, $\mathbf{u}_\Delta$ (Noack *et al.*, 2003) (defined as the first POD mode of the Gaussian time-filtered field $\mathbf{u}-\mathbf{U}$),

$$\mathbf{u}_B(\mathbf{x},t) = \mathbf{U}(\mathbf{x}) + a_\Delta(t)\mathbf{u}_\Delta(\mathbf{x}) \tag{2}$$

The periodic fluctuations, $\mathbf{u}_\phi(\mathbf{x},t)$, are represented as an expansion of N_h empirical harmonic modes. Each harmonic consists of a pair of complementary modes that have either symmetry (even harmonics) or anti-symmetry (odd harmonics) with respect to the geometrical plane of symmetry, $y=0$. Symmetric and anti-symmetric modes will be denoted with superscripts 's' and 'a', respectively. For example, the 1st harmonic mode pair is denoted $\mathbf{u}_1^a$ and $\mathbf{u}_2^a$, or as a single complex mode $\tilde{\mathbf{u}}_1 = \mathbf{u}_1^a - i\mathbf{u}_2^a$. The second harmonic is $\tilde{\mathbf{u}}_2 = \mathbf{u}_1^s - i\mathbf{u}_2^s$, and so on. These modes are determined using the POD of the velocity fluctuation $\mathbf{u}-\mathbf{u}_B$ such that the periodic fluctuations may be written as functions of these modes or fluctuation amplitudes, A_n, and phases, $n\phi$, of each harmonic,

$$\begin{aligned}\mathbf{u}_\phi(\mathbf{x},t) &= \sum_{n=1}^{N_a}(a_{2n-1}^a\mathbf{u}_{2n-1}^a + a_{2n}^a\mathbf{u}_{2n}^a) \\ &\quad + \sum_{n=1}^{N_s}(a_{2n-1}^s\mathbf{u}_{2n-1}^s + a_{2n}^s\mathbf{u}_{2n}^s) \\ &= \sum_{n=1}^{N_h}\Re\left[A_n e^{in\phi(t)}\tilde{\mathbf{u}}_n\right].\end{aligned} \tag{3}$$

where the total number of harmonics in the expansion is equal to the sum of the anti-symmetric (odd) and symmetric (even) harmonics $N_h = N_a + N_s$. The remaining term, $\mathbf{u}_S(\mathbf{x},t)$, is the remaining stochastic fluctuation (unresolved residual) of the decomposition.

DYNAMIC-STOCHASTIC MODEL

A Galerkin projection of the Navier-Stokes equations onto the five mode velocity field expansion (eq. 1), with $\mathbf{u} = \sum_i^5 a_i\mathbf{u}_i$ where $\mathbf{u}_1 = \mathbf{u}_1^a$, $\mathbf{u}_2 = \mathbf{u}_2^a$, $\mathbf{u}_3 = \mathbf{u}_1^s$, $\mathbf{u}_4 = \mathbf{u}_2^s$, $\mathbf{u}_5 = \mathbf{u}_\Delta$, and a_i the corresponding amplitudes, yields the following set of ODEs (Holmes *et al.*, 2012).

$$\frac{\mathrm{d}a_i}{\mathrm{d}t} = c_i + \sum_{j=1}^{5} l_{ij}a_j + \sum_{j,k=1}^{5} q_{ijk}a_j a_k, \quad i = 1,\ldots,5. \tag{4}$$

The strongest limitation of eq. 4 which remains consistent with the empirical POD observations of the planar PIV measurements follow the form

$$a_1^a = A_1\cos(\omega_1^* t) \tag{5a}$$
$$a_2^a = A_1\sin(\omega_1^* t) \tag{5b}$$
$$a_1^s = A_2\cos(2\omega_1^* t + \tau) \tag{5c}$$
$$a_2^s = A_2\sin(2\omega_1^* t + \tau) \tag{5d}$$
$$a_\Delta = B_{\mathrm{FP}} + B' \tag{5e}$$

where A_1, A_2, B' and ω_1^* are slowly varying functions of time as compared to the oscillation period $T_1 = 2\pi/\omega_1^*$. The constant B_{FP} is chosen so that $\mathbf{U} + B_{\mathrm{FP}}\mathbf{u}_\Delta$ represents the fixed point of the Navier-Stokes equation, *i.e.*, for which the amplitude of the modes are zero, $\{a_i = 0\}$.

Closely following a generalized mean-field model derivation (Noack *et al.*, 2003; Luchtenburg *et al.*, 2009), the following stochastic-deterministic dynamical model is found

$$\frac{\mathrm{d}a_1^a}{\mathrm{d}t} = (\sigma_1 - \beta_1 B' + \beta_\xi\xi)a_1^a - (\omega_1 + \gamma_1 B')a_2^a \tag{6a}$$
$$\frac{\mathrm{d}a_2^a}{\mathrm{d}t} = (\sigma_1 - \beta_1 B' + \beta_\xi\xi)a_2^a + (\omega_1 + \gamma_1 B')a_1^a \tag{6b}$$
$$\frac{\mathrm{d}a_1^s}{\mathrm{d}t} = (\sigma_2 - \beta_2 B')a_1^s - (2\omega_1 + 2\gamma_1 B')a_2^s + h_1^s \tag{6c}$$
$$\frac{\mathrm{d}a_2^s}{\mathrm{d}t} = (\sigma_2 - \beta_2 B')a_2^s + (2\omega_1 + 2\gamma_1 B')a_1^s + h_2^s \tag{6d}$$
$$\frac{\mathrm{d}B'}{\mathrm{d}t} = \sigma_\Delta B' + c_1 A_1^2 \tag{6e}$$
$$\frac{d\xi}{dt} = -\sigma_g\xi + n(t). \tag{6f}$$

This is a two-harmonic oscillator system augmented by a Langevin equation (eq. 6f) with a Gaussian noise term $n(t)$ leading to a Wiener process, $\xi(t)$. The first harmonic is self-excited with growth-rate $\sigma_1 - \beta_1 B'$ and frequency $\omega_1 + \gamma_1 B'$. The growth-rate is damped by the base-flow amplitude B' and modulated by the Wiener process, $\xi(t)$, which accounts for the source/sink effect of the stochastic term, $\mathbf{u}_S$, in eq. 1.

The second harmonic is a damped oscillator with growth-rate $\sigma_2 - \beta_2 B' < 0$ and the frequency $2\omega_1 + 2\gamma_1 B'$, driven by the quadratic forcing terms

$$h_1^s = f[(a_1^a)^2 - (a_2^a)^2] + 2ga_1^a a_2^a, \tag{7a}$$
$$h_2^s = -g[(a_1^a)^2 - (a_2^a)^2] + 2fa_1^a a_2^a. \tag{7b}$$

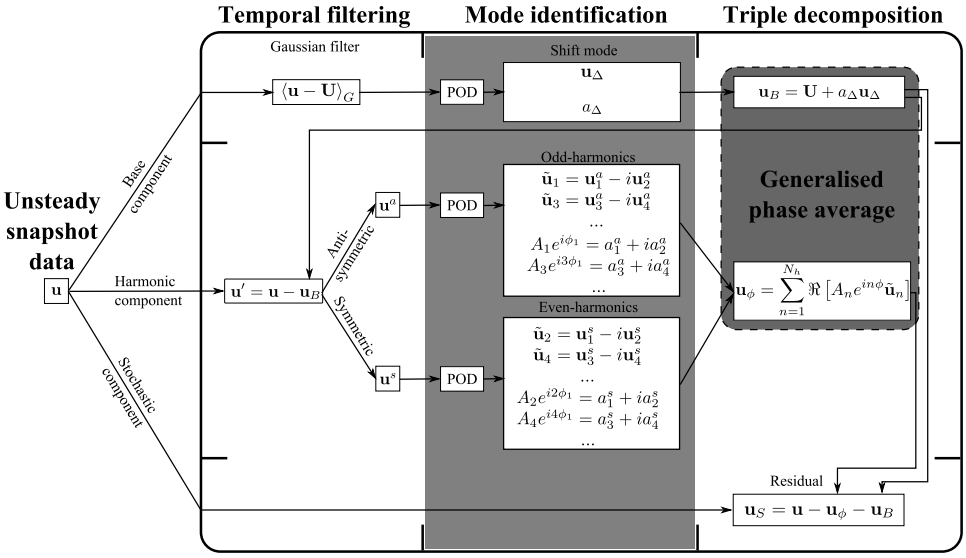

Figure 1. Flow chart for generalized phase average processing.

The base-flow is described by eq. 6e, and following Noack *et al.* (2003); Luchtenburg *et al.* (2009), its slow variation can be exploited, reducing to the algebraic relationship

$$a_\Delta = B_{FP} + c_1 A_1^2. \tag{8}$$

The coefficients σ_1, σ_2, β_1, β_2, β_ξ, ω_1, γ_1, σ_g, f, g, B_{FP}, and c_1 are calibrated empirically based on the state $\{a_i\}$ determined by generalized phase averaging of unsteady flow data following Luchtenburg *et al.* (2009).

EXPERIMENTAL SETUP

The generalized phase average is undertaken on a set of PIV measurements conducted in the University of Calgary wind tunnel. Horizontal (x-y) and vertical (x-z) planes (see Fig. 2 for coordinate system and schematic) were measured in the wake of the wall-mounted square cylinder, installed in a blow-down open-test-section wind tunnel. A LaVision FlowMaster high-frame-rate particle image velocimetry (PIV) system is used with a pulse separation of 50μs and frame rates of 500 Hz (capturing 4 to 5 data points per shedding cycle). This planar data is used to generate a 3D construction of the coherent structures in the wake.

Test conditions were a free-stream velocity, $U_\infty = 15$ m/s, a Reynolds number $Re = U_\infty d/\nu = 12{,}000$, a free-stream turbulence intensity of 0.8%, and an aspect ratio of the square cylinder of $h/d = 8$, mounted with one face normal to the flow. The vortex shedding Strouhal number was found to be $St = fd/U_\infty = 0.102 \pm 0.003$. The turbulent boundary layer originates at the leading-edge of the mounting plate. Two boundary layers with thickness $\delta/d = 0.72$ and 2.6 (at the cylinder mounting location with the cylinder removed) were investigated.

For the 3D flow reconstruction, 6 simultaneous surface pressure measurements at $z/h = \{0.25, 0.50, 0.75\}$ on either side of the cylinder were correlated with the flow state observed from POD of the PIV data. Using techniques described in Bourgeois (2012); Bourgeois *et al.* (2013), the pressure data is correlated with the velocity field POD modes and a prediction scheme is used to estimate the 3D

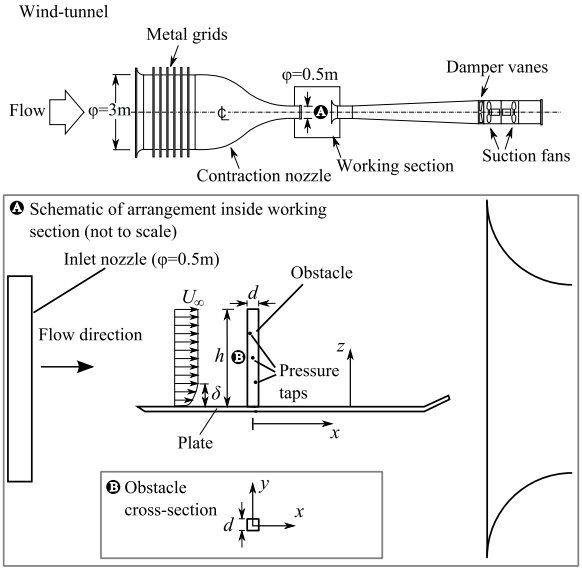

Figure 2. Schematic of experimental configuration.

coherent flow at any instant given the surface pressure. The methodology is similar to remote sensing techniques (Borée, 2003; Taylor & Glauser, 2004). The sampling rate for the surface pressure is 10.24 kHz and is synchronized with the PIV measurements using a TTL trigger.

RESULTS

Figure 3 depicts the 3D topology of the shed vortex skeletons, for an arbitrary phase and identified using the λ_2-criterion, based on the reconstructed flow in the wake of an aspect ratio 8 cylinder for $\delta/d = 0.72$ and 2.6. Briefly, while the two topologies are anti-symmetric, corresponding to a staggered *von Kàrmàn-like* arrangement of counter-rotating shed vortices, dynamically important near-wall differences are evident. Whereas the thicker boundary layer case is characterized by a chain of interconnecting counter-rotating ring structures, the thinner case generates half-ring structures interconnected on the free-end side, but with the near-wall vortex cores diverting outwards suggesting strong

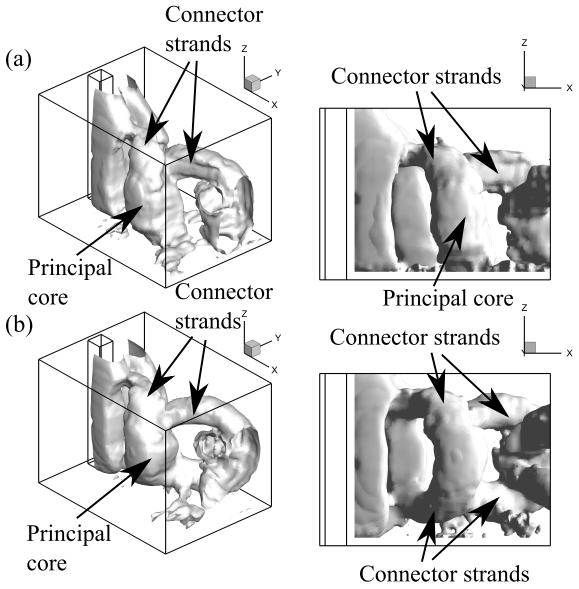

Figure 3. Coherent structures identified by λ_2.

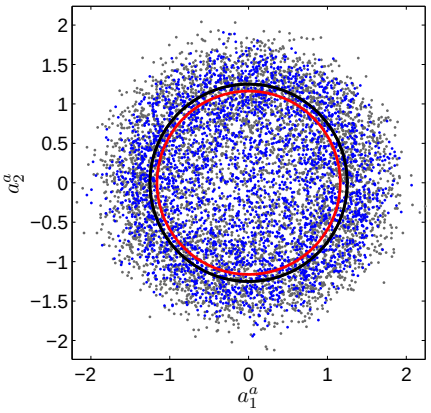

Figure 4. State observed from the fundamental harmonic mode pair ($\delta/d = 0.72$: blue; $\delta/d = 2.6$: grey) and the phase averaged amplitude ($\delta/d = 0.72$: red; $\delta/d = 2.6$: black). Plane: $z/d = 4$.

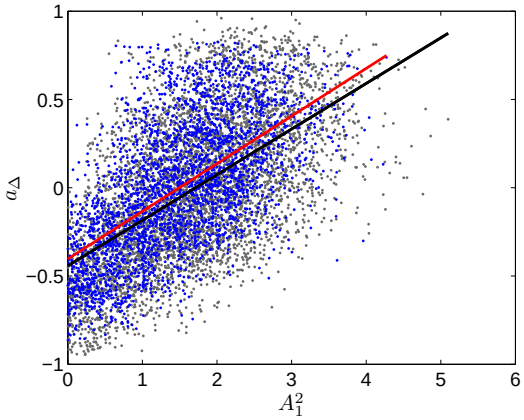

Figure 5. Amplitude and shift mode state observed ($\delta/d = 0.72$: blue; $\delta/d = 2.6$: grey) and regression of the mean field paraboloid curve ($\delta/d = 0.72$: red; $\delta/d = 2.6$: black). Plane: $z/d = 4$.

interactions with the wall flow. The flow physics of the vortex shedding for the two cases are interesting, but the focus here is on the improved dynamical representation provided by the generalized phase average over traditional means.

Despite the differing spatial flow structure, the temporal behaviour of the respective modes, $a_i(t)$, captured by the generalized phase average is similar. In both cases, the dominant (most energetic) fluctuations are represented by the 1^{st} and 2^{nd} harmonic pairs and the slow-drift mode, thus conforming well to eqs. 5. Although the stochastic model constants for each case differ, the form of the model describing their dominant modal dynamics is the same (see also the case of the $h/d = 4$ wake where the technique was first applied, Bourgeois *et al.*, 2013). Hence, the generalized phase average is a robust data reduction method for increased dynamical resolution of the 3D turbulent shedding phenomenon across parameter changes (e.g., h/d, δ/d).

Focusing on the results of the plane $z/d = 4$ for the two boundary layers, the amplitude of the oscillatory modes, $A_1 = \sqrt{(a_1^a)^2 + (a_2^a)^2}$, over time is far from constant in both cases (see Fig. 4). Large amplitude excursions are found, as shown by the instantaneous data points of phase and amplitude shown in Fig. 4 (from projection of the PIV data onto the harmonic mode pair POD eigenfunctions). The traditional phase averaged amplitude is shown as solid lines in the figure. Clearly, a richness of dynamic information on the coherent motion is lost when considering the behaviour on the limit cycle only.

The identification of the relationship of the instantaneous oscillatory and shift mode amplitudes by the generalized phase average supports that mean field theory developed for laminar flows (Noack *et al.*, 2003) holds at least approximately (within some stochastic deviation) for fully turbulent wakes as seen in Fig. 5. This theory describes how slow variations of the base flow are coupled to the variations in the oscillatory mode amplitude through the mean field paraboloid (eq. 8 derived from the Galerkin projection of the Navier-Stokes equations).

The degree the oscillation amplitude modulation, and the coupled changes in the base flow through the shift mode, is quite high in the studied wakes. The standard deviation of the amplitude is more than 30% of the mean amplitude for the plane $z/d = 4$. These aspects (modulated fluctuation amplitude and base flow) of the flow are therefore particularly important for a low residual description of the coherent structures, or conversely, for maintaining a high-fidelity resolution of the coherent energetic content independently of the fluctuation amplitude and base flow modulations.

The mean square residuals, normalized by the mean square fluctuation, is given by:

$$Z := \frac{\int_\Omega (\mathbf{u} - \hat{\mathbf{u}}) \bullet (\mathbf{u} - \hat{\mathbf{u}})\, dA}{\int_\Omega \mathbf{u}'' \bullet \mathbf{u}''\, dA} = \frac{\|\mathbf{u} - \hat{\mathbf{u}}\|_\Omega^2}{\overline{\|\mathbf{u}''\|_\Omega^2}} \qquad (9)$$

where $\mathbf{u}$ is the PIV data, $\hat{\mathbf{u}}$ is the estimate according to the phase average (either generalized or traditional), and $\mathbf{u}'' = \mathbf{u} - \mathbf{U}$. This residual represents the ratio of the unresolved to total fluctuation energy.

As expected, the mean squared residuals of the two descriptions (traditional and generalized phase average) are similar when the oscillation amplitude is close to its mean (*i.e.* near the limit cycle), however, instantaneous residuals are typically 30 to 40% of the mean fluctuation level

higher for the phase averaged description when amplitudes deviate from the mean amplitude (Fig. 6). The generalized phase average, meanwhile, has roughly constant residuals over the range of observed oscillation amplitudes. The residual level is an estimation of the unresolved fluctuation energy. The present observations imply that for increasing deviations from the limit-cycle, the traditional phase average yields an increasingly poorer resolution of the coherent motion, whereas the estimations obtained with generalized phase average are independent of the state in the low-order space. Therefore, the generalized phase average provides a superior descriptive framework for the dynamics.

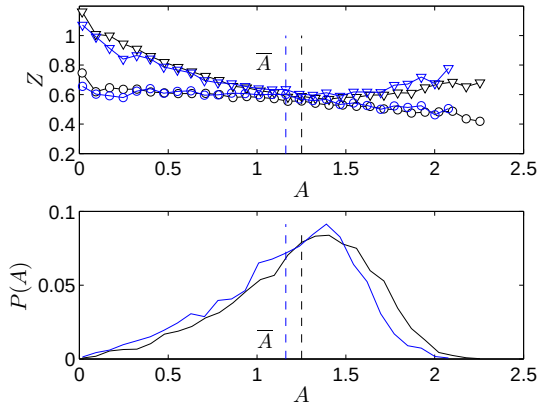

Figure 6. Normalized residual, Z, of the phase averaged (triangles) and generalized phase average (circles) and probability density, P. Blue: $\delta/d = 0.72$; black: $\delta/d = 2.6$. Plane: $z/d = 4$.

Using the correlations of the velocity modes with the pressure field allows for 3D flow estimations and application of the generalized phase averaging to the 3D field. The flow state observations were used to calibrate the stochastic model described by eqs. (6 - 8). The integration of this model is portrayed in Fig. 7 (black line) which displays a good agreement with the observations (grey points).

The filtered behaviour that the pressure estimated flow field (with a state corresponding to the grey points behind the model solution trajectory in Fig. 7) provides a clear illustration of the benefits of the generalized phase average over the harmonic oscillations captured by the traditional phase average, namely the modulated fluctuation amplitudes, $A_1(t)$ and $A_2(t)$, and the intimately linked base flow modulation described by $a_\Delta(t)$. The 3D data shows a clear parabolic relationship between the base flow amplitude, a_Δ, and that of the fundamental harmonic together with a stochastic fluctuation associated with higher-order mode interactions. In the low-order system, the stochastic contributions are modelled with the Langevin equation modulating only the fundamental harmonic amplitude. Notwithstanding, the behaviour along the mean-field paraboloid and the 1^{st} harmonic phase plot are well rendered for both cases. When comparing the two wakes, the observed wider amplitude fluctuation range for the thicker relative to the thinner boundary layer case is also rendered. Note that in the chosen plane $z/d = 4$, the structures are least distorted (see Fig. 3) and it is expected that the differences between the two cases are quantitative rather than qualitative.

The second harmonics and baseflow are subsequently coupled to this modulation and interact through the linear and quadratic mode-interaction terms of eqs. 6–8. This approach is well-justified for both cases when comparing the observed and modelled phase portraits linking the 1^{st} and 2^{nd} harmonics in Fig. 7. The two cases show significant qualitative differences. The second harmonic is associated with the dynamics of the connector strands, which display distinct structures as observed from Fig. 3.

The pressure-velocity correlations found from each set of simultaneous PIV planar and surface pressure measurements provides a preprocessing scheme which subsequently acts as a means for 3D flow estimation from pressure data. As such, the estimated flow field loses some of the stochastic behaviour observed in Figs. 4 and 5.

This low-order representation and its associated model presents the next most-significant modal and inter-mode dynamics of the vortex shedding wake (and other analogous systems), and offers the next step on the path of increasing complexity that turbulent coherent structures display.

CONCLUDING REMARKS

This study outlines a generalized phase average decomposition applicable to a wide range of turbulent flows with oscillatory dynamics. This technique is used to extract the two typical shed vortex topologies found in the wake of a wall-mounted square-cylinder depending on the boundary layer thickness, δ/d. The oscillation and base flow amplitude are highly modulated (30% standard deviation relative to the mean is common) and thus the generalized description is preferred over the traditional description in order to appropriately describe the flow over the range of conditions observed. The fact that these modulations are analytically coupled, approximately obeying the mean field paraboloid, further supports the analytical inclusion of time varying amplitude and base flow parts since they portray a highly coherent and repeatable behaviour which should be accounted for in low-order representations. These strengths are ultimately demonstrated through a six-dimensional stochastic reduced order model of the wake flow.

REFERENCES

Borée, J. 2003 Extended proper orthogonal decomposition: a tool to analyse correlated events in turbulent flows. *Exp. Fluids* **35**, 188–192.

Bourgeois, J. A. 2012 Three-dimensional topology and dynamical modelling of vortex shedding from finite surface-mounted bluff bodies. PhD thesis, University of Calgary.

Bourgeois, J. A., Noack, B. R. & Martinuzzi, R. J. 2013 Generalised phase average with applications to sensor-based flow estimation of the wall-mounted square cylinder wake. *Submitted J. Fluid Mech* .

Bourgeois, J. A., Sattari, P. & Martinuzzi, R. J. 2011 Alternating half-loop shedding in the turbulent wake of a finite surface-mounted square cylinder with a thin boundary layer. *Phys. Fluids* **23** (095101), 1–15.

Holmes, P., Lumley, J. L. & Berkooz, G. 2012 *Turbulence, Coherent Structures, Dynamical Systems and Symmetry, 2nd Ed.*. Cambridge University Press.

Liu, J. T. C. 1989 Coherent structures in transitional and turbulent free shear flows. *Ann. Rev. Fluid Mech.* **21**, 285–315.

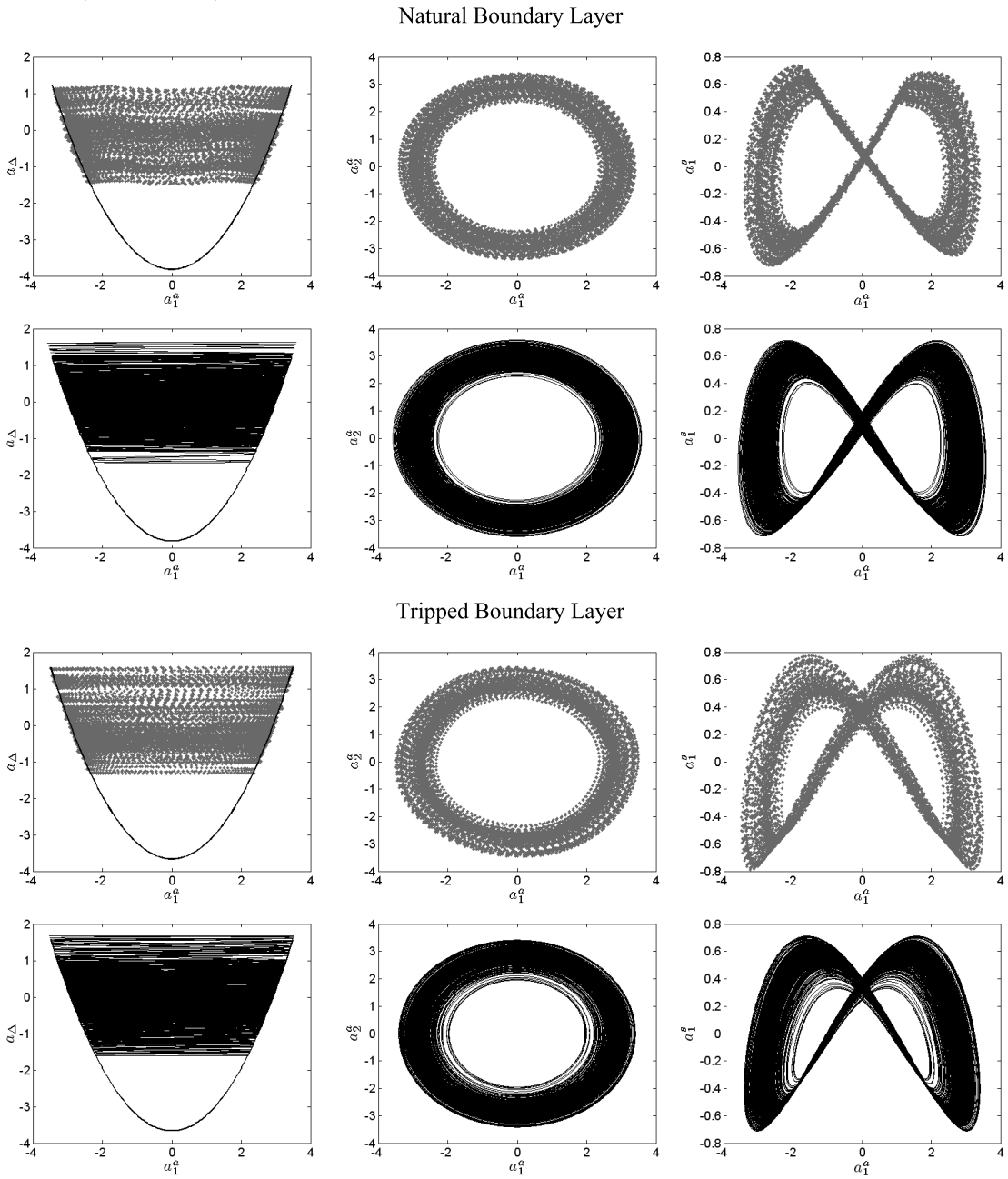

Figure 7. Stochastic model of the generalized phase average system (black) of the 3D estimated flow field and the observed system state (grey points) for the body wake with $\delta/d = 0.72$ (Top) and $\delta/d = 2.6$ (Bottom). Left to right: zeroth, first, and second harmonic over a_1^a. The mean field paraboloid is superimposed over a_Δ.

Luchtenburg, D. M., Günter, B., Noack, B. R., King, R. & Tadmor, G. 2009 A generalized mean-field model of the natural and actuated flows around a high-lift configuration. *J. Fluid Mech.* **623**, 283–316.

Noack, B. R., Afanasiev, K., Morzyński, M., Tadmor, G. & Thiele, F. 2003 A hierarchy of low-dimensional models for the transient and post-transient cylinder wake. *J. Fluid Mech.* **497**, 335–363.

Oberleithner, K., Sieber, M., Nayeri, C. N., Paschereit, C. O., Petz, C. Hege, H.-C., Noack, B. R. & Wygnanski, I. 2011 Three-dimensional coherent structures in a swirling jet undergoing vortex breakdown: stability analysis and empirical mode construction. *J. Fluid Mech.* **679**, 383–414.

Rowley, C. W. & Williams, D. R. 2006 Dynamics and control of high-Reynolds number flows over open cavities. *Ann. Rev. Fluid Mech.* **38**, 251–276.

Sumner, D., Heseltine, J. L. & Dansereau, O. J. P. 2004 Wake structure of a finite circular cylinder of small aspect ratio. *Exp. Fluids* **37**, 720–730.

Taylor, J. A. & Glauser, M. N. 2004 Towards practical flow sensing and control via POD and LSE based low-dimensional tools. *Journal of Fluids Engineering* **126**, 337–345.

Wang, H. F., Zhou, Y., Chan, C. K. & Lam, K. S. 2009 Momentum and heat transport in a finite-length cylinder wake. *Exp. Fluids* **46**, 1173–1185.

Williamson, C. H. K. 1996 Vortex dynamics in the cylinder wake. *Annu. Rev. Fluid Mech.* **28**, 477–539.